Available online at www.sciencedirect.com
ScienceDirect
Nuclear Instruments and Methods in Physics Research B 256 (2007) 319–323
NIM B Beam Interactions with Materials & Atoms
www.elsevier.com/locate/nimb

Transport and STM measurements of HCI modified materials

J.M. Pomeroy [a,*], H. Grube [a], A.C. Perrella [a,b,c], C.E. Sosolik [d], J.D. Gillaspy [a]

[a] Atomic Physics Division, National Institute of Standards and Technology, 100 Bureau Dr., Gaithersburg, MD 20899-8421, USA
[b] School of Applied and Engineering Physics, Cornell University, Ithaca, NY, USA
[c] Nano-electronics Team, US Army Research Laboratory, Adelphi, MD, USA
[d] Department of Physics and Astronomy, Clemson University, Clemson, SC, USA

Available online 2 February 2007

Abstract

While more than a decade of work has provided glimpses into the physics of highly charged ion (HCI) neutralization on surfaces, two prominent objectives remain unfulfilled: (1) a unified, quantitative model for separating the kinetic energy response of a wide range of materials classes from the effects of HCIs' potential energy effects and (2) insertion of HCI technology(s) as a cost-effective processing tool in a high-volume market sector. The National Institute of Standards and Technology (NIST) electron beam ion trap (EBIT) facility has recently incorporated tools for preparing clean, atomically flat surfaces of single crystals from gold to tungsten to silicon and for depositing and patterning thin films that range from high resistivity oxides to transition metals like cobalt and nickel. Current activities are focused on utilizing this unique capability to simultaneously address both of the objectives above by employing technologically important magnetic multi-layer systems to perform transport measurements that provide new insight into the fundamental processes that occur during HCI–surface neutralization. Specifically, we are producing Magnetic Tunnel Junctions (MTJs) critical to both magnetic devices and incorporating HCIs in the processing recipe to adjust critical electronic properties that are currently inhibiting their advancement. In return, the electrical response of the tunnel junction to the HCI processing provides a novel approach to performing ensemble measurements of HCI–surface interactions. By varying the construction of the tunnel junction, critical tests of the role of electron density, densities of states and electronic structure in the HCI–surface charge exchange can be performed.
© 2006 Elsevier B.V. All rights reserved.

PACS: 68.37.Ef; 61.80.Jh; 75.70.Cn; 81.40.Wx

Keywords: Highly charged ions; Scanning tunnelling microscopy; Gold; Magnetic tunnel junction; Tungsten; Mica; Nano-feature; EBIT

1. Introduction

The interactions of highly charged ions (HCIs) with materials has been a matter of much interest but rather limited investigation largely due to the difficulty of producing HCIs and clean surfaces in the same facility. Measurements of enormous secondary electron, secondary ion and sputtered atom yields suggest that the large neutralization energies carried by HCIs drive new physics during surface interactions, e.g. [1,2] and references therein. Supplementing this work, scanning probe images of HCI irradiated surfaces have revealed unique nanofeatures formed by single ions on surfaces like graphite, mica, LiF, sapphire and SiO_2 (e.g. [3–5]). Satisfactory reconciliation of all the available data under a single model and the broader objective of harnessing these effects for technological benefit remain elusive and motivate further HCI-materials studies.

Recent studies of HCI modified materials at the NIST electron beam ion trap (EBIT) facility can be categorized into two classes: (1) preparation, irradiation and scanning tunneling microscopy/spectroscopy (STM/S) imaging and spectroscopy of surfaces (Section 3) and (2) using HCI irradiation as a processing step in a multilayer system that is engineered to maximize sensitivity to HCI interactions (Section 4). The next section briefly updates the capabilities and techniques used at the NIST EBIT for preparing and

* Corresponding author.
E-mail address: joshua.pomeroy@nist.gov (J.M. Pomeroy).

0168-583X/$ - see front matter © 2006 Elsevier B.V. All rights reserved.
doi:10.1016/j.nimb.2006.12.019

irradiating samples. Finally, following a summary of recent data, a brief discussion and overall summary is presented in Section 5.

2. Experimental system

The NIST EBIT facility has been described at various times since its inception and evolution, thus many of the technical details may be found elsewhere [6,7]. For the casual reader, the NIST EBIT can produce HCIs as high as Bi^{81+} in the current configuration (ionization energies up to 30 keV) that may be trapped and manipulated for spectroscopic observation or transported via an ion beam line to study HCI matter interactions, either gas or solid phase. Xenon is the most commonly studied ion species; 10 pA of Xe^{44+} or 25 pA of Xe^{25+} is typical.

Recently, the materials preparation capabilities for HCI-solid phase experiments have been improved and warrant a brief introduction. A system of independent vacuum chambers with a sample interchange system are attached at the end of the beam line: (1) a high vacuum (base pressure $P_b \approx 5 \times 10^{-6}$ Pa) load–lock for introducing up to four samples (or STM probes) that is also equipped for plasma oxidation; (2) an ultra-high vacuum (UHV) target chamber ($P_b \approx 3 \times 10^{-8}$ Pa, $\approx 2 \times 10^{-7}$ Pa during sample irradiation) with ion current measurement and ion beam imaging systems; (3) a UHV surface preparation and analysis chamber ($P_b \approx 8 \times 10^{-9}$ Pa) with a commercial scanning probe microscope, surface preparation and in vacuum sample storage; and a UHV materials deposition chamber ($\approx 2 \times 10^{-7}$ Pa during deposition) equipped with multi-pocket electron beam evaporation, microbalance thickness monitoring and shadow masking. Additional pertinent details will be provided as they apply to different experiments. All the samples were prepared and imaged *in situ* except for the gold on mica experiment (samples were transported in atmosphere to Clemson University and imaged using a commercial variable temperature UHV STM system) and the ballistic electron emission microscopy (BEEM) imaged magnetic tunnel junctions (MTJs) (samples were transported in low vacuum to Cornell University where the samples were characterized).

3. STM images of HCI irradiated surfaces

Presented in Fig. 1 are three STM images from different samples after exposure to HCIs. The topmost image in Fig. 1 is an example of one of three types of features observed on Au(1 1 1) (single crystal 1 cm diameter $\times \approx 6$ mm thick) after exposure to HCIs. Sample preparation involves sputtering using 3 keV Ar ions and annealing to 700 °C many iterations to produce atomically flat terraces with a step every 100 nm on average. The hexagonal pyramid shown is due to a single Xe^{44+} ion's impact with ≈ 8 keV/q (q is the ion charge) on the clean surface, imaged *in situ* within 2 h of exposure to HCIs. In addition to simple hexagons, hexagonal rings and hexagons with one or more

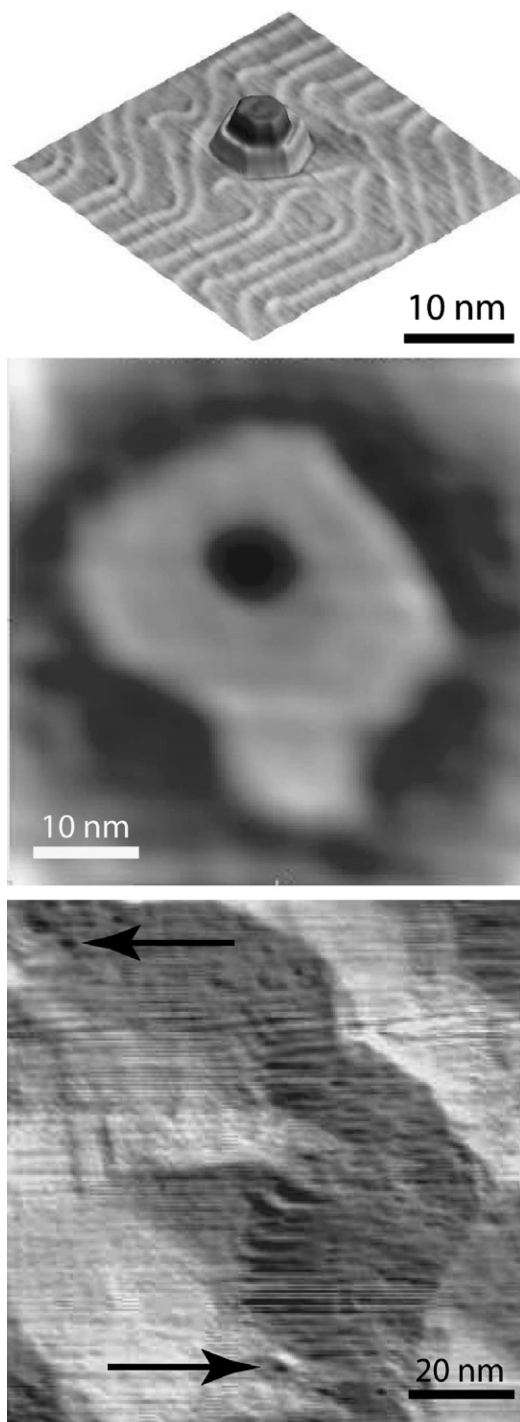

Fig. 1. STM images of features formed by single HCIs: (top) a simple two monolayer high hexagon on Au(111) from Xe^{44+} – full image 32 nm × 32 nm; (middle) a one monolayer high hexagonal ring on gold coated mica from Xe^{25+} – full image 50 nm × 50 nm; (bottom) subtle vacancy features (arrows) observed on W(1 0 0) from Xe^{25+} – full image 100 nm × 100 nm, presented as derivative.

adjacent pits have also been observed. The hexagonal shape is a consequence of the relaxation of the displaced atoms to match the symmetry of the underlying surface. In series of images like the image shown, vacancies percolating up in the region surrounding the hexagon have been

observed and suggest that the material that formed the pyramid may have been displaced from deep within the crystal. As a general rule, however, the number of vacancies observed in the STM images account for only a fraction of the volume of displaced mass.

The middle image in Fig. 1 is similar to the top except that the sample is 150 nm of gold deposited on a mica substrate (≈8 mm × 8 mm), which was transported to Clemson University in air for imaging after HCI exposure. In this image, the ion-impact feature from a Xe^{25+} ion is a large hexagonal ring with a hole in the middle that is interpreted as the ion's point of entry. This feature is similar to features observed on the single crystal gold surface.

The bottom image in Fig. 1 presents two examples of a class of subtle features that were observed on a W(1 0 0) single crystal sample after the sample was exposed to Xe^{25+}, the image presented is the derivative to increase contrast. The starting surface in this system was an array of square mounds with an average center to center spacing of about 50 nm and heights of several nanometers (achieving an atomically flat surface was not possible with the equipment available at the time of the experiment). The features appear as ≈3 nm diameter divots at a density consistent with the ion density. While these features are less dramatic than features in the top and middle frames, they were only observed in images following HCI irradiation. No debris flows were observed in this system, possibly due to the high density of steps that could easily carry the adatoms away from the impact site despite the low overall diffusivities.

Additionally, complex extreme ultraviolet lithography (EUVL) multilayer mirrors terminated in ruthenium and then exposed to air were exposed to HCIs ranging from Xe^{10+} to Xe^{44+}. Samples were scanned with STM/S and later imaged with focussed 13.4 nm EUV light to map the surface reflectivity (the surface reflectivity is very sensitive to the Ru capping layer thickness). The results show that the reflectivity is changed by HCIs substantially more than can be reasonably explained by kinetic sputtering alone. Tunnelling spectroscopy of the mirror surface shows a marked increase in the surface density of states as a function of charge state that is consistent with the removal of the native oxide and suggestive of neutralization energy dependence. A more extensive description is reported elsewhere [8].

4. HCI modified multilayers

In the second class of experiments (engineered systems maximized for HCI susceptibility), tunnel junctions utilizing aluminum oxide barriers were prepared and exposed to HCIs. Aluminum oxide is a material that already has a demonstrated ''potential sputtering'' susceptibility [9]. Devices are formed by depositing (lower) electrodes capped with an aluminum oxide tunnel junction. The aluminum oxide surface is then exposed to a controlled density of HCIs which presumably form depleted zones of a few nm^2 that may be completely ablated, or perhaps just weakened or thinned.

Since the HCI modified interface is buried in subsequent processing, it is neither possible to measure the same device before and after exposure, nor is it possible to image the ''modified'' oxide layer in a conventional sense. However, BEEM (described in detail elsewhere [10]) can provide a spatial map of the ballistic (unscattered) current flow injected by the tip through the system of layers. BEEM is a variant of STM (which maintains a constant tunnel current and therefore height between tip and sample) that also collects current from beneath a Schottky barrier integrated into the sample (e.g. a gold–silicon interface). The Schottky barrier allows only unscattered electrons to be transmitted, so the lower current channel generates a transmission map as the tip is rastered.

Shown in Fig. 2 is a BEEM image of an MTJ device with an integrated Schottky barrier that was exposed to HCIs after completion of the aluminum oxide layer (the complete layer structure is inset in the lower left). After HCI exposure, the device was transferred through air (briefly) to a low vacuum ''suitcase'' and returned to Cornell where the upper electrodes were deposited and it was imaged. The three bright patches seen conduct as much as 20 times the current of the surrounding region and have not been observed in any unexposed samples. The size of the patches is consistent with features observed in other materials systems and the feature density is consistent with the applied dose.

While the sample in Fig. 2 was prepared and imaged at Cornell, numerous MTJ samples have now been prepared completely *in situ* at NIST. Silicon chips with 1 μm of thermal oxide (insulating) are introduced into the vacuum system and then transferred to the deposition chamber. Materials are then deposited through a shadow mask placed <1 mm from the sample face to form ≈40 μm wide

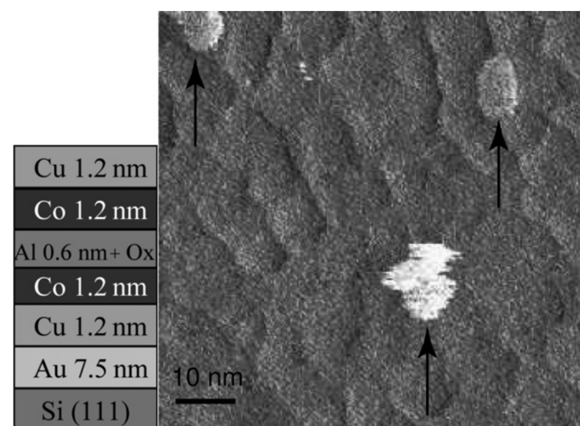

Fig. 2. Ballistic electron emission microscopy (BEEM) image of a completed magnetic tunnel junction (MTJ) whose tunnel barrier has been exposed to Xe^{44+} – full image 100 nm × 100 nm. The three bright patches (arrows) carry more than ten times the current of the surrounding areas. These patches are interpreted as regions thinned or ablated by HCI erosion of the aluminum oxide. The MTJ layer structure is inset lower left.

lower leads. A second mask (or no mask) is then used to deposit aluminum for the tunnel barrier. The sample is then transferred to a small chamber used to plasma oxidize the aluminum (expansion ratio ≈1.4), followed by exposure to HCIs. Finally, the samples are completed by depositing ≈80 μm wide upper leads through a third mask that results in four cross shaped devices (≈3200 μm^2) per chip; two top leads and two lower leads per device. A circuit is formed by passing current from one lower electrode, through the tunnel junction and into an upper electrode to measure the junction properties; the second upper and lower leads are used to probe the voltage (4 point geometry).

Shown in Fig. 3 is data from twelve chips with a few different aluminum layer thicknesses and different oxidation processes that result in different effective barrier thicknesses. One device on each chip was left unexposed as a control and the other three were exposed to different doses of Xe^{44+}. Lines connect devices from the same chip. These samples demonstrate a systematic increase in the sample conductance with HCI dose that can be modelled simply as

$$\sigma_f = \sigma_i + N\sigma_{chan}, \tag{1}$$

where σ_f is the measured conductance, σ_i is the conductance due to the undamaged barrier, N is the number of ion channels per device and σ_{chan} is the mean conductance per HCI channel. The data have been adjusted by a constant offset to compensate for differences in σ_i, which is approximately dose independent. Assuming each HCI forms a single quantum conduction channel of 3.88×10^{-5} S per spin, the data would follow the dashed line in the upper part of the plot. In the case that two overlapping HCI impacts are needed per conduction quanta, the data would follow the dashed line near the bottom of the plot.

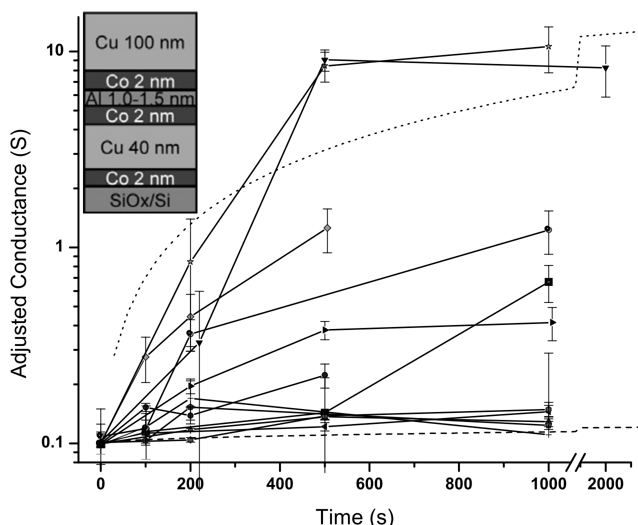

Fig. 3. Adjusted conductivities of MTJ devices exposed to ≈1 pA/mm^2 of Xe^{44+} as a function of the aluminum oxide layer's exposure time. The MTJ layer structure is inset upper left, pre-oxidized aluminum thicknesses vary for different devices plotted between 1.0 nm and 1.5 nm. Further discussion provided in the text.

5. Discussion

Images of HCI induced features on free electron metals are presented, including single crystal gold, gold on mica and tungsten. The gold data show a significant amount of displaced mass (>1000 atoms per HCI) and large penetration holes. Monitoring of single features for several hours revealed vacancies percolating to the surface suggesting that some of the displaced mass originates from deep in the crystal, but the observed vacancies do not account for the total displaced mass. On the tungsten surface, observed features are similar to the penetration holes on gold, but without the material outflows. The difference may be due to the higher binding energies in tungsten, or may be simply due to the much higher step edge densities that can easily distribute material. Although this work demonstrates for the first time that HCIs can form nanofeatures on metals, additional work is required to definitively establish the degree to which potential energy is the source of the feature formation.

BEEM images of ion irradiated MTJs show high conductivity patches 10 nm to 20 nm across and transport measurements on similar MTJs show a systematic increase in the conductance with HCI dose. Most of the transport measurement data fall below the curve for creating a single quantum conduction channel per ion, but above the curve for two ions hitting the same place and forming a conduction quanta. This suggests that the barrier thicknesses used are near the threshold for completely breaking through the barrier and many ion impacts may only be thinning the oxide. Refinement of the sample processing to allow more precise control of the barrier's ion susceptibility is in progress.

References

[1] T. Schenkel, A.V. Hamza, A.V. Barnes, D.H. Schneider, Interaction of slow, very highly charged ions with surfaces, Prog. Surf. Sci. 61 (2–4) (1999) 23.
[2] F. Aumayr, H. Winter, Potential sputtering, Philos. Trans. R. Soc. Lond. 362 (2004) 77.
[3] C. Ruehlicke, M.A. Briere, D. Schneider, AFM studies of a new type of radiation defect on mica surfaces caused by highly charged ion impact, Nucl. Instr. and Meth. B 99 (1–4) (1995) 528.
[4] D.C. Parks, M.P. Stockli, E.W. Bell, L.P. Ratliff, R.W. Schmieder, F.G. Serpa, J.D. Gillaspy, Non-kinetic damage on insulating materials by highly charged ion bombardment, Nucl. Instr. and Meth. B 134 (1) (1998) 46.
[5] I.C. Gebeshuber, S. Cernusca, F. Aumayr, H.P. Winter, AFM search for slow MCI-produced nanodefects on atomically clean monocrystalline insulator surfaces, Nucl. Instr. and Meth. B 205 (2003) 751.
[6] J. Gillaspy, Highly charged ions, J. Phys. B: At. Mol. Opt. Phys. 34 (2001) R93.
[7] A. Pikin, C. Morgan, E. Bell, L. Ratliff, J. Gillaspy, A beam line for highly charged ions, Rev. Sci. Instr. 67 (1996) 2528.
[8] J.M. Pomeroy, L.P. Ratliff, J.D. Gillaspy, S. Bajt, Potential energy sputtering of EUVL materials, in: V. Bakshi (Ed.), EUV Sources for

Lithography, SPIE – The Interantional Society for Optical Engineering, Bellingham, WA, p. 1033.
[9] G. Hayderer, S. Cernusca, M. Schmid, P. Varga, H.P. Winter, F. Aumayr, D. Niemann, V. Hoffmann, N. Stolterfoht, C. Lemell, L. Wirtz, J. Burgdorfer, Kinetically assisted potential sputtering of insulators by highly charged ions, Phys. Rev. Lett. 86 (16) (2001) 3530.
[10] L.D. Bell, W.J. Kaiser, M.H. Hecht, L.C. Davis, New electron and hole spectroscopies based on ballistic electron-emission microscopy, J. Vac. Sci. Technol. B 9 (2) (1991) 594.